Understanding Hydrocarbon Adsorption in the UiO-66 Metal–Organic Framework: Separation of (Un)saturated Linear, Branched, Cyclic Adsorbates, Including Stereoisomers

ARTICLE *in* THE JOURNAL OF PHYSICAL CHEMISTRY C · MAY 2013

Impact Factor: 4.77 · DOI: 10.1021/jp402294h

7 AUTHORS, INCLUDING:

Tim Duerinck
Northwestern University
20 PUBLICATIONS **132** CITATIONS
SEE PROFILE

Frederik Vermoortele
University of Leuven
37 PUBLICATIONS **1,256** CITATIONS
SEE PROFILE

Sofia Calero
Universidad Pablo de Olavide
164 PUBLICATIONS **3,112** CITATIONS
SEE PROFILE

Joeri F M Denayer
Vrije Universiteit Brussel
209 PUBLICATIONS **4,699** CITATIONS
SEE PROFILE

THE JOURNAL OF PHYSICAL CHEMISTRY C

Article

pubs.acs.org/JPCC

Understanding Hydrocarbon Adsorption in the UiO-66 Metal–Organic Framework: Separation of (Un)saturated Linear, Branched, Cyclic Adsorbates, Including Stereoisomers

T. Duerinck,[†] R. Bueno-Perez,[‡] F. Vermoortele,[§] D. E. De Vos,[§] S. Calero,[‡] G. V. Baron,[†] and J. F. M. Denayer*[,†]

[†]Department of Chemical Engineering, Vrije Universiteit Brussel, Pleinlaan 2, 1050 Brussel, Belgium

[‡]Department of Physical Chemical & Natural Systems, Universidad Pablo de Olavide, Seville 41013, Spain

[§]Center for Surface Chemistry and Catalysis, Katholieke Universiteit Leuven, Kasteelpark Arenberg 23, 3001 Leuven, Belgium

Supporting Information

ABSTRACT: The low coverage adsorption properties of alkanes, alkenes, and aromatics of the linear, branched, and cyclic type (ca. 70 molecules) were studied using inverse pulse gas chromatography at zero coverage on the zirconium metal–organic framework UiO-66 and its functionalized analogues UiO-66-Me, UiO-66-NO_2, UiO-66-Me_2 in the temperature range 433–573 K. In our study, we determined and analyzed the adsorption enthalpy, Henry constants, and entropic factors. Preferential adsorption of bulky molecules is observed with specific adsorbate and cage size effects, yielding very specific, preferential adsorption. Remarkably high adsorption selectivity factors (up to 14) for cyclo- compared to *n*-alkanes were found. The presence of additional groups (methyl, nitro) on the linkers in the framework influences adsorption properties significantly, mainly by reducing the effective pore size. Whereas increased selectivity is observed for UiO-66-Me, this effect decreases again upon addition of a second methyl group, UiO-66-Me_2. The latter allows for tuning confinement factors inside the pores, thus adsorption properties of the metal–organic framework. The selective adsorption results from the interaction in the smallest octahedral cage. The extreme confinement in the tetrahedral cage allows for stereoselective separation of disubstituted cycloalkanes and *cis*/*trans* alkenes. Monte Carlo simulations were performed for the unfunctionalized UiO-66 framework. First, a comparative study between the force fields Dreiding and UFF is performed with *n*-alkanes to obtain accurate and reproducible values. The simulations show adsorbate molecular size–adsorbent cage size effects similar to window/cage effects reported for zeolites (e.g., silicalite). Second, adsorption properties were simulated for selected cases, including stereoisomers. Careful analysis of the adsorbate's molecular positioning in the framework confirms the experimental data. The framework's selectivity results from adsorption in the tetrahedral cage at zero coverage. Furthermore, simulations show important contributions of entropic factors to the observed adsorption selectivity.

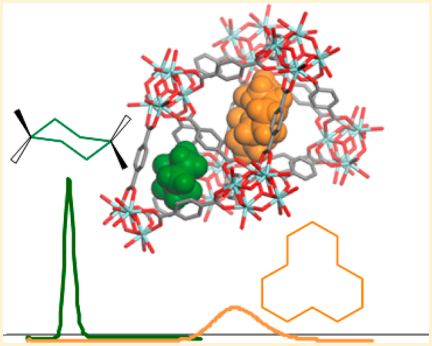

1. INTRODUCTION

Micro- and mesoporous materials are well-known for their excellent adsorption properties in terms of capacity and selectivity. These materials (zeolites, silica, active carbon, etc.) have found their application in industry for separation, purification, or catalytic purposes. One of the extremely challenging key operations in industry remains the molecular separation and purification of stereoisomers.[1] Such mixtures require complex and application type specific conditions. For example, production of cycloalkyl fragments, common substructures in pharmacological substances,[2] or specialty chemicals[3] such as liquid crystals,[4] often involves stereoisomer purification. Classical separation techniques only offer mediocre results, rely on the use of complex mobile and stationary phase compositions in HPLC conditions, and are cost intensive.[5] Separation via preferential adsorption of specific isomers in porous materials could provide a cost-effective alternative. Among these porous material types, metal–organic frameworks (MOFs) have received much attention in the past decade.[6] The combination of metal clusters (as cornerstones) and organic building blocks (as linkers) offers a potential limitless number of possible structures. The synthesis of large numbers of these structures has been reported. MOFs were investigated in adsorption or catalytic studies or modeled by a variety of methods.[7] Some MOFs with specific topologies have been reported as potential candidates for stereoselective separations.[1a,c,8] Computational screening offers a tool to make a preliminary selection based on theoretical predictions and known structures.[9] However, limited experimental evidence has yet been given that such separations can be achieved in practice, with the exception of homochiral frameworks.[10]

Received: March 6, 2013
Revised: May 17, 2013
Published: May 23, 2013

In this paper, we report on the adsorption and stereoselective properties of the Zr-MOF UiO-66 and its structural analogues UiO-66-Me, UiO-66-NO_2. Cavka et al. reported the original synthesis of UiO-66, UiO-67, and UiO-68 materials based on the inorganic brick $Zr_6O_4(OH)_4$ and 1,4-benzene-dicarboxylate (BDC) as an organic linker for UiO-66.[11] Isoreticular synthesis and incorporation of modified BDC linkers in the framework were reported for a variety of functionalities including amides, amino, nitro, halogen, alkyl, sulfonic, etc.[12] The crystal and particle size of the UiO-66 material can be controlled by modulated synthesis.[13] The polarity of the structure can be changed by employing modified linkers. The effect of linker functionality is illustrated by reduced 30% water adsorption reduction on UiO-66-Me_2,[14] increased CO_2 uptake in the presence of sulfonic acid groups,[12b] or changing selectivity in catalysis.[15] The native UiO-66 is relatively hydrophobic as it adsorbs little water (<5 mol/kg) below a relative humidity of 20% followed by a steep step to 20 mol/kg which is likely due to pore filling. Water adsorption affinity and capacity are comparable to SBA-1 or BPL carbon materials.[14b] The complex structure of small tetrahedral (~7.5 Å) and large octahedral (~11 Å) cages was elucidated by a combination of X-ray diffraction (XRD), NMR, spectrometry, and computational optimizations.[16] Upon dehydroxylation of $Zr_6O_4(OH)_4$ to Zr_6O_6, the electrostatic potential lowers near the zirconium oxide cluster. This results in a significant structure distortion. The effective size of the microporous windows appears to be temperature dependent due to the rotational motion of the benzene rings.[17] Furthermore, the UiO-66 framework shows remarkable thermal, chemical, and mechanical stability.[11,14b,16a] The potential of the UiO-66 framework was evaluated experimentally and computationally for gas based applications (H_2, CH_4, CO_2, etc.).[12g,18] No specific interaction sites were found for CH_4 on the native UiO-66 material in simulations, but specific interactions between CO_2 and polar functionalities were observed In humid conditions, CO_2 uptake remains unchanged.[19] Incorporation of UiO-66-NH_2 in polymer membranes increased the CO_2 permeability in CO_2/CH_4 separations.[20] Enhanced affinity of the dimethyl functionalized UiO-66 for CO_2 was reported.[21] Reversed shape selectivity in the adsorption of hexane and xylene isomers in vapor and liquid phase on columns packed with UiO-66 has been reported.[22] A follow-up study using capillary GC confirmed this and extended it to alkylbenzenes.[23] These studies already revealed the interesting adsorption properties of UiO-66.

In this paper, we characterized the adsorption properties of UiO-66 type MOFs by determining adsorption parameters of ca. 70 molecules on four different UiO-66 materials (UiO-66, UiO-66-Me, UiO-66-Me_2, UiO-66-NO_2) using pulse gas chromatography. Adsorption trends for alkanes, alkenes, and aromatic molecules in the C_4–C_{12} range are extensively discussed. The adsorption properties of alkanes and other small hydrocarbons have often been studied in order to understand the properties and adsorption mechanisms of porous media.[24] More specifically, low coverage adsorption properties on zeolites,[25] silica,[26] porous carbon,[27] and MOFs[28] were reported. Comprehensive reviews on this topic were published in the MOF special issue of *Chemical Reviews*.[7] Furthermore, we have demonstrated the potential of the UiO-66 framework for stereoselective separations. The experimental data are supplemented with extensive Monte Carlo simulations. The simulation part consists of a comparative study of the UFF and Dreiding force fields, followed by the modeling of adsorption trends for linear and cyclic alkanes.

2. MATERIALS AND METHODS

2.1. Material Synthesis and Pulse Gas Chromatography. UiO-66 and functionalized variants (UiO-66-Me, UiO-66-Me_2, UiO-66-NO_2) were synthesized according to published methods.[15a] The structure was verified by XRD (Figure S1, Supporting Information). Pulse chromatographic experiments were performed using a set ca. 70 probe molecules. The tested molecules are listed in Tables 1 and S1. Adsorption equilibrium

Table 1. List of Adsorbates of Which the Adsorption Properties Were Measured at Zero Coverage on One or More Adsorbents: UiO-66, UiO-66-Me, UiO-66-Me_2, and UiO-66-NO_2

n-pentane	2,3-dimethylheptane	1-octene
n-hexane	2,2,4-trimethylpentane	1,7-octadiene
n-heptane	2,2,4-trimethylhexane	1-nonene
n-octane	2-methylbutadiene	1-decene
n-nonane	cyclopentane	*trans*-5-decene
n-decane	cyclohexane	1-dodecene
n-undecane	cycloheptane	cyclohexene
n-dodecane	cyclooctane	1-methylcyclohexene
2-methylbutane	cyclodecane	3-methylcyclohexene
2-methylpentane	cyclododecane	4-methylcyclohexene
2-methylhexane	*trans*-1,4-dimethylcyclohexane	1-methylcyclohexadiene
2-methylheptane	*cis*-1,4-dimethylcyclohexane	*cis*-cyclooctene
2-methyloctane	*cis*-1,3-dimethylcyclohexane	*cis*-/*trans*-cyclododecene
3-methylpentane	*trans*-1,3-dimethylcyclohexane	benzene
3-methylhexane	trans-1,2-dimethylcyclohexane	toluene
3-methylheptane	*cis*-1,2-dimethylcyclohexane	ethylbenzene
3-methylnonane	methylcyclopentane	*o*-xylene
4-methylheptane	methylcyclohexane	*p*-xylene
4-methylnonane	ethylcyclohexane	*m*-xylene
2,2-dimethylbutane	1-hexene	propylbenzene
2,3-dimethylbutane	*cis*-2-hexene	mesitylene
2,3-dimethylpentane	*trans*-2-hexene	isopropylbenzene
2,4-dimethylpentane	*cis*-3-hexene	2-chlorotoluene
3,3-dimethylpentane	*trans*-3-hexene	benzylchloride
2,2-dimethylhexane	1-heptene	chlorobenzene
2,4-dimethylhexane	*trans*-2-heptene	cyclohexanol
2,5-dimethylhexane	*cis*-2-heptene	

Henry constants were calculated from the first moment of the chromatographic response curves in the range of 200–300 °C for UiO-66, 200–300 °C for UiO-66-Me, 200–280 °C for UiO-66-NO_2, and 160–260 °C for UiO-66-Me_2. It was shown that the experiments were performed in the linear part of the isotherm by injecting different amounts (Figure S2). Absence of diffusion limitations was confirmed by using different carrier flow rates. A detailed explanation of the experimental setup and procedure was previously reported.[29]

2.2. Monte Carlo Simulations. The adsorption properties of UiO-66 were simulated using Monte Carlo techniques. The Lennard–Jones parameters for UiO-66 were retrieved from the work of Goddart et al.[30] The adsorbate molecules were modeled using the united atom force field parameters of the TraPPE set.[31] Linear alkanes were modeled as flexible

dx.doi.org/10.1021/jp402294h | J. Phys. Chem. C 2013, 117, 12567–12578

molecules and cyclic molecules as rigid units. The structures of the cyclic molecules used for the simulations represent the conformers of minimal energy. These were taken from the literature[39] or directly calculated by structure optimization and validated by comparison with literature data on molecular energy levels when available. It is noteworthy to keep in mind that only 1 conformer is taken in account, while a distribution of conformers may be present at experimental conditions, depending on the experimental temperature. As a check, adsorption of the chair and twisted-boat conformations of cyclohexane was modeled. Identical values (within error margins) for enthalpy and entropy factors were obtained.

The adsorption enthalpy and entropy at zero coverage were calculated using the Widom test particle method. The simulation was run till computed values were equilibrated and calculation errors were below 1%. During the initial phase, two force fields were tested: UFF and Dreiding. Both force fields yielded results close to the experimental data. The Universal Force Field (UFF) was chosen for further modeling as computation time was lower to obtain similar error margins. The number of cycles used is 200 000 for C_2−C_4, 500 000 C_5−C_6, and 3 000 000 for C_7 and up for linear alkanes, and 1 000 000 for the cyclic molecules. The preferential adsorption site of the adsorbate at zero coverage was investigated by simulating the case of exactly one molecule in NVT ensemble, Monte Carlo Simulations with only 100 000 cycles allowing the following moves: insertion, reinsertion, translation, and rotation. The actual molecular position was verified by either plotting the center of mass or visual inspection of the molecule in the simulation box. An overview of the simulated properties is given in Table S3.

3. RESULTS AND DISCUSSION

3.1. Pulse Gas Chromatography. The chromatograms of the injected components show relatively symmetrical peaks at the different experimental temperatures and for small and large molecules. Since the first-order moment was independent of injection volume for injection volumes between 0.01 and 0.04 μL, it could be concluded that experiments were performed in the linear part of the adsorption isotherm. No change in pressure drop or retention time was observed for the duration of the experiments (3−4 months), indicating the pellet's integrity. In Figure 1, this is demonstrated for *n*-octane, cyclohexene, ethylbenzene, and 3,3-dimethylpentane on UiO-66. A complete overview of the obtained Henry constants, adsorption enthalpy, entropy, and pre-exponential factors for ca. 70 different molecules is given in Table S1. The adsorption enthalpy for a subset of commonly studied adsorbates (e.g., *n*-alkanes, cyclohexane, benzene, xylenes, etc.) is given in Table 2.

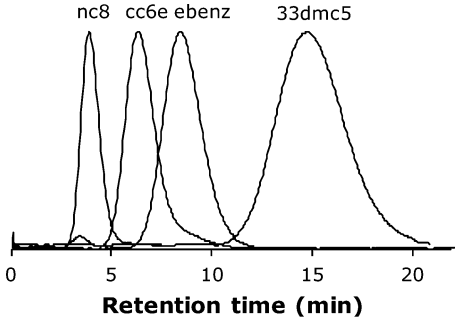

Figure 1. Normalized chromatographic profile of *n*-octane, cyclohexene, ethylbenzene (ebenz), and 3,3-dimethylpentane on UiO-66 at 523 K.

The retention of *n*-alkanes on UiO-66, UiO-66-Me, UiO-66-Me_2, and UiO-66-NO_2 is well in line with theoretical behavior in the Henry region. van't Hoff plots correlate (r^2 > 0.997) nearly perfect with linear regression within the measured temperature range. Figure 2 shows the van't Hoff plot for *n*-alkanes on UiO-66-Me.

3.1.1. Influence of the Linker Functionality. The four differently functionalized UiO-66 materials show distinctively different adsorption properties as illustrated by the plot of pre-exponential factors K'_0 and Henry constants K'_{523} at 523 K by carbon number N_c for *n*-alkanes on all four materials. In general, larger adsorption constants are obtained for the functionalized (-Me, -Me_2, -NO_2) materials. A stronger interaction between adsorbed molecules and framework is witnessed for functionalized UiO-66 (Figures 3−5). The main effect for pre-exponential factors and adsorption enthalpy is the reduction of effective pore size by introduction of an additional functional group on the organic linker, leading to enhanced dispersive interactions and a decrease in molecular freedom. This observation is in line with the work Yang et al.[16a,18f] They reported that the chemical environment inside the framework's cages is influenced by the chemical nature of the functional group on the BDC linker. No specific interaction sites were found for CH_4 on the native UiO-66 material in simulations, but specific interactions between CO_2 and polar functionalities were observed. In the series UiO-66, UiO-66-Me, and UiO-66-Me_2, adsorption properties change stepwise with the number of methyl groups present on the organic linker (Figure 5). The change in enthalpy value for *n*-alkanes between UiO-66 and UiO-66-Me_2 is larger than between UiO-66 and UiO-66-Me but not systematically twice as large. Henry constants for C_7−C_{10} *n*-alkanes are 2−8% larger for UiO-66-Me and 21−29% larger for UiO-66-Me_2 compared to UiO-66. The influence of the nitro group on the BDC linker allows for less straightforward interpretation. Both the effect of effective pore size reduction and a change in polar character of the framework need to be considered. The effective size reduction of the pores is similar, yet a bit smaller than that of a single methyl group. The respective van der Waals volumes for the bonded nitro and methyl groups are 55 Å^3 and 61 Å^3. However, pre-exponential factors for C_5−C_8 *n*-alkanes are relatively lower on UiO-66-NO_2 than with UiO-66-Me. The electronic effect is perhaps most pronounced in the Henry constant values (shown at 523 K in Figure 3) for *n*-alkanes. Here UiO-66-NO_2 has increasingly different properties: Henry constants' values for *n*-pentane to *n*-octane are 1.5−2.0 times larger than those of UiO-66 and the methyl functionalized analogues, with a distinctive increase to a factor of ca. 4 for *n*-octane and *n*-decane. Although differences for a subset of molecules may be pronounced, no general trend is visible when considering (unsaturated) branched and cyclic alkanes as well. Figure 4 shows the compensation plot of adsorption enthalpy and pre-exponential factors for the four different materials. It is clear that each of the materials has distinctive properties. The unfunctionalized UiO-66 material falls well off the other materials trend. The presence of an additional group on the organic linkers leads to a broader pattern of data points, thus more overlap. In the left visualization, some UiO-66 variants dominate the graph as more data points were recorded. The figure on the right gives a more representative view. Here the adsorption enthalpy is plotted as a function of the adsorbate's molecular weight. The

dx.doi.org/10.1021/jp402294h | J. Phys. Chem. C 2013, 117, 12567−12578

Table 2. Experimental Adsorption Enthalpy (kJ/mol) for *n*-Alkanes, Cycloalkanes, and Aromatics on UiO-66 Materials[a]

molecule	UiO-66	UiO-66-Me	UIO-66-NO_2	UiO-66-Me_2
n-pentane	−54.8 ± 0.6	−56.0 ± 1.3	−60.2 ± 1.3	−59.8 ± 0.7
n-hexane	−56.2 ± 0.7	−62.7 ± 1.4	−67.0 ± 1.4	−65.3 ± 0.7
n-heptane	−59.4 ± 0.7	−66.3 ± 1.4	−72.4 ± 1.1	−73.0 ± 0.8
n-octane	−64.4 ± 0.7	−73.2 ± 1.5	−77.4 ± 1.6	−84.1 ± 1.0
n-nonane	−72.5 ± 1.6	−83.1 ± 1.7	−88.8 ± 2.7	−93.9 ± 1.5
n-decane	−79.5 ± 1.7	−95.6 ± 2.8	−99.4 ± 4.4	−101.3 ± 2.4
n-undecane		−103.0 ± 7.9		−109.5 ± 5.2
n-dodecane	−90.5 ± 2.4	−110.4 ± 8.4		
cyclopentane	−50.4 ± 1.7	−59.3 ± 1.3		−62.0 ± 0.7
cyclohexane	−59.9 ± 0.7	−71.2 ± 1.5	−68.4 ± 1.5	−72.4 ± 1.2
cycloheptane	−74.7 ± 1.6	−83.9 ± 1.7	−74.7 ± 2.4	−82.5 ± 1.3
cyclooctane	−79.3 ± 2.0	−90.1 ± 1.8	−82.9 ± 6.7	−87.4 ± 2.1
cyclodecane		−98.2 ± 5.8		−109.5 ± 5.2
cyclododecane	−84.3 ± 1.9			
benzene	−51.6 ± 0.7	−62.7 ± 1.4	−61.4 ± 1.4	
toluene	−58.2 ± 1.2	−71.2 ± 2.0	−67.6 ± 2.2	
ethylbenzene	−63.9 ± 1.4	−80.1 ± 1.6	−76.9 ± 3.0	
o-xylene	−66.2 ± 1.5	−85.1 ± 1.7	−82.4 ± 2.6	
p-xylene	−58.7 ± 1.4	−77.7 ± 1.6	−78.4 ± 2.4	
m-xylene	−59.2 ± 1.4	−79.6 ± 1.6	−78.8 ± 2.4	
propylbenzene	−68.0 ± 1.5	−83.2 ± 1.7	−87.2 ± 2.6	
mesitylene	−64.7 ± 1.4	−80.8 ± 1.6	−97.9 ± 2.9	
isopropylbenzene	−67.9 ± 2.4	−86.3 ± 1.7	−85.5 ± 2.6	

[a]Full data set can be found in Supporting Information, Table S2.

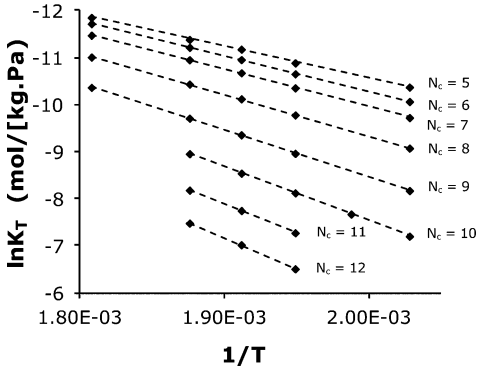

Figure 2. The van't Hoff plots for linear alkanes (C_5−C_{12}) on UiO-66-Me show linear evolution (r^2 > 0.9996) of pre-exponential factors ln K_T with the inverse temperature ($1/T$).

ratio adsorption enthalpy/molecular weight is ca. 0.6 for UiO-66 and above 0.7 for the functionalized materials. It is clear that several molecules lie off the general trend in the case of UiO-66-Me and UiO-66-NO_2. These data points represent cyclic or double branched compounds. Size and shape effects play a significant role in this and will be discussed later.

Within the studied data set, a substantial subset of alkenes and aromatic compounds is present. Figure 6 shows the adsorption enthalpy values for C_6 isomers on the UiO-66, UiO-66-Me, and UiO-66-NO_2 materials. Nearly identical adsorption enthalpies (∼0−2 kJ/mol) were obtained for 1-alkenes compared to *n*-alkanes for UiO-66 and UiO-66-NO_2 whereas on average a somewhat increased interaction (>3 kJ/mol) is seen for UiO-66-Me. This observation indicates that the polar nature of the nitro group does not significantly increases the enthalpic interaction with the double bond but that the reduction in effective pore size is much more important. Aromatic molecules have a lower enthalpic interaction than

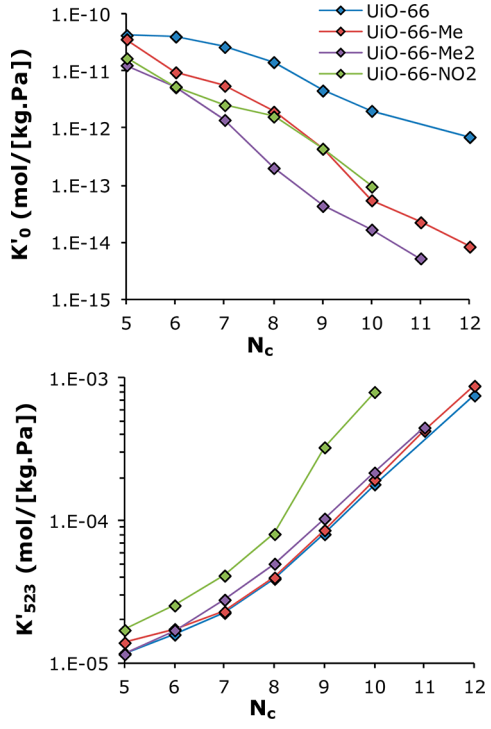

Figure 3. Experimental pre-exponential factor K'_0 (top) and Henry constants K'_{523} (bottom) of *n*-alkanes on UiO-66, UiO-66-Me, UiO-66-NO_2, and UiO-66-Me_2 plotted versus N_c. Errors fall within the symbols.

their cycloalkenes or unsaturated analogues. An increasing degree of unsaturation decreases the enthalpic interactions. The Henry constants are 10−30% lower for alkylcycloalkenes and 50−60% lower for aromatic molecules compared to structurally analogue alkanes.

dx.doi.org/10.1021/jp402294h | J. Phys. Chem. C 2013, 117, 12567−12578

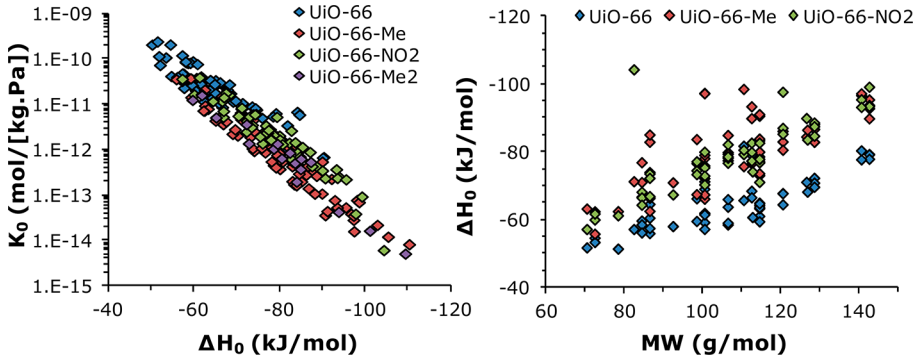

Figure 4. (Left) Compensation plot of experimental pre-exponential factors K'_0 and adsorption enthalpy ΔH_0 visualizing all data points. (Right) Experimental adsorption enthalpy ΔH_0 as a function of molecular weight MW for identical data sets.

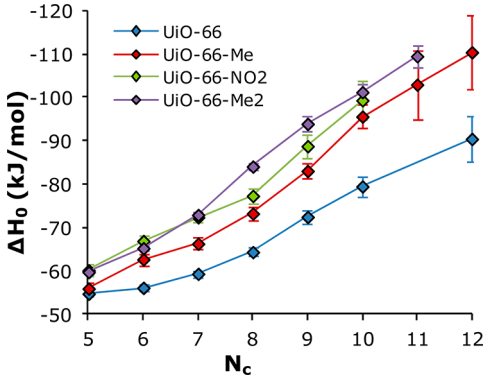

Figure 5. Experimental adsorption enthalpy ΔH_0 of *n*-alkanes as a function of carbon number.

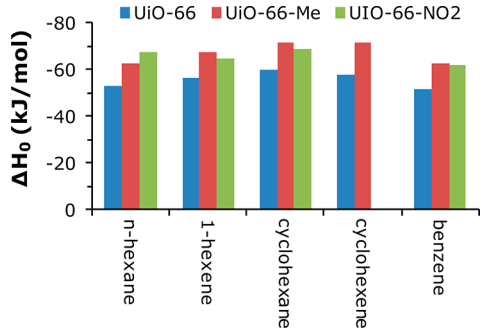

Figure 6. Experimental adsorption enthalpy values for C6 isomers on UiO-66, UiO-66-Me, and UiO-66-NO_2.

An interesting case study is to look at the subset of alkylcyclohexanes, alkylcyclohexenes, and alkylaromates. Not only influence of unsaturated bonds but also enthalpic and steric effects may be distinguishable. From the given example of methylcyclohexane, methylcyclohexene, and toluene (Table 3), it can be denoted that although the adsorption selectivity of methylcyclohexane over *n*-heptane differs between UiO-66, UiO-66-Me, and UiO-66-NO_2, selectivity for toluene over *n*-heptane is nearly identical for these materials. A stepwise decrease in preferential adsorption selectivity (compared to *n*-heptane) with increasing number of unsaturated bonds is observed for UiO-66-Me. A preferential adsorption of *o*-xylene over ethylbenzene (α = 1.4−1.5), *m*-xylene (α = 1.6−1.9), and *p*-xylene (α = 1.4−2.2) is found for all UiO-66 materials. This observation is in line with a previous study by Barcia et al.[22a]

Table 3. Experimental Separation Factor (Ratio of Henry Constants) for Alkylcyclo-C_6 over *n*-Heptane at 523 K

molecule	UiO-66	UiO-66-Me	UiO-66-NO_2
methylcyclohexane	6.0	5.7	4.0
1-methylhexene	2.7	4.0	4.0
toluene	2.5	2.6	2.4

3.1.2. Size and Shape Effects. A good way to identify shape selective adsorption from differences based on physicochemical parameters, such as boiling point, is to plot the retention (here expressed as Henry constants at 523 K) as a function of vapor pressure.[26c] In the case of nonselective adsorption, a linear trend is expected, and *n*-alkanes, isoalkanes, and cycloalkanes are expected to fall on one line. In the case of the UiO-66 materials, no linear trend can be identified (Figures 7 and S5−S6), not even for *n*-alkanes, with a pronounced different trend for cyclic alkanes. In general, branched alkanes fall in between the linear and cyclic trend with the exception of 2,2-dimethylbutane, 2,3-dimethylbutane, and 3,3-dimethylpentane. The molecules have a densely branched structure and resemble more a spherical unit than a long chain. Adsorption selectivity branched/linear is within the 3.3−6.9 range. The adsorption strength per carbon number is on average 3−4 kJ/mol stronger than the *n*-alkane for UiO-66 and UiO-66-Me with a limited elevation of ca. 1 kJ/mol for UiO-66-NO_2. With respect to hexane isomer separations, similar tendencies were found as in the work of Barcia et al.[22a]

3.1.2.1. Branched Alkanes. In comparison to previous works on MOFs such as MIL-47,[28e] amino-MIL-53,[28c] and zeolites,[25b,c,32] no linear dependence of the adsorption enthalpy with chain length elongation is observed for *n*-alkanes on UiO-66. The difference in adsorption enthalpy between N_C and N_{C-1} is −1.4 kJ/mol between *n*-pentane and *n*-hexane, −3.2 for *n*-hexane and *n*-heptane, −5.0 kJ/mol for *n*-heptane and *n*-octane, with a maximum of −8.1 kJ/mol for *n*-octane and *n*-nonane after which it decreases again. Similar tendencies are observed for all studied materials with maxima of 12.5 kJ/mol between *n*-nonane and *n*-decane for UiO-66-Me, 11.6 kJ/mol between *n*-nonane and *n*-decane for UiO-66-NO_2, and 11.1 kJ/mol between *n*-heptane and *n*-octane. The deviation of linear chain length dependency is most pronounced for C_7−C_9 alkanes as depicted in Figure 5. Considering molecular size and the different cages in the framework, this coincides with the fact that *n*-hexane still fits nicely in the smallest, tetrahedral cage.

At lower carbon numbers, the monobranched alkanes are preferentially adsorbed over the linear alkanes, with separation factors to 2.9 (Table S2). The preferential adsorption of

dx.doi.org/10.1021/jp402294h | J. Phys. Chem. C 2013, 117, 12567−12578

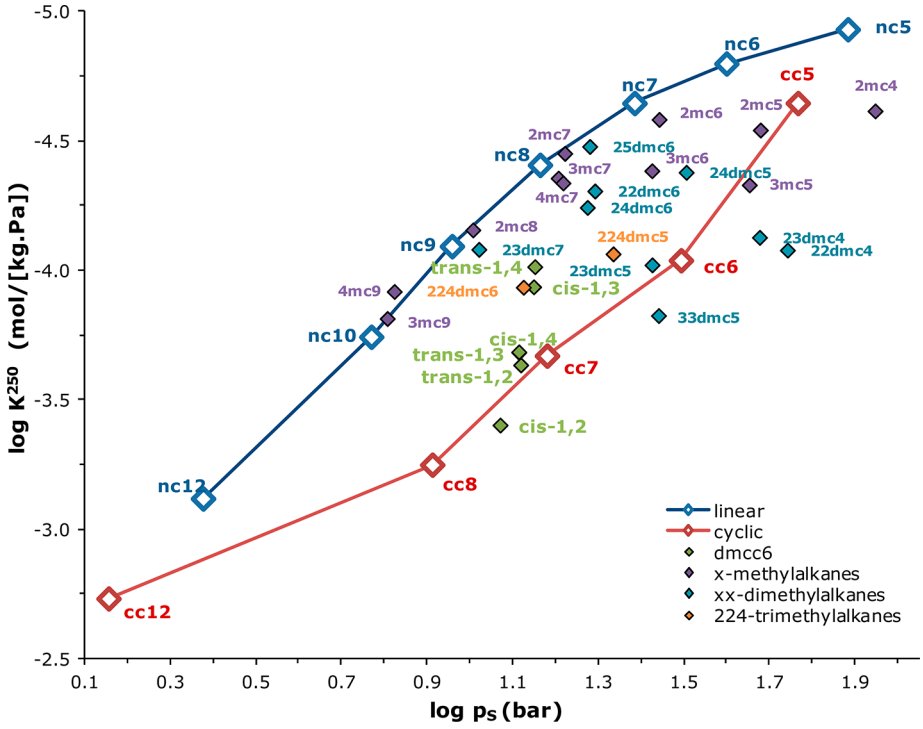

Figure 7. Relationship between logarithm of the experimental Henry constant and vapor pressure of alkanes for UiO-66 at 523 K.

branched *n*-alkanes, called "inverse shape selectivity", is quite unusual and has been observed in only a few cases (e.g., SAPO-34,[33] SAPO-5,[34] MCM-22,[25e] and ZIF-96[35]). Most porous materials tend to preferentially adsorbed linear chains compared to branched ones. This selective adsorption of monobranched alkanes on UiO-66 strucures nearly vanished for C_{7-8} ($\alpha \sim 1$) and even inverses for longer chains ($\alpha < 1$ for C_{9-10}) (Table S2). In the case of double or triple branched alkanes, this inverse shape selectivity effect is stronger, with a distinctive contribution of isoalkyl groups at beginning and end of the carbon chain. For example, 3,3-dimethylpentane adsorbs nearly 7 times more than *n*-heptane on UiO-66 and UiO-66-Me at 523 K. The difference in adsorption enthalpy between *n*-heptane and 3,3-dimethylpentane is respectively 12 and 31 kJ/mol. The strong preference for double branched, bulky components in combination with increased enthalpic interaction supports the hypothesis of a confinement effect.

3.1.2.2. Cycloalkanes. Remarkably, cyclic molecules are interacting strongly with all of the tested UiO-66 variants (Tables 2 and 4). Other microporous adsorbents, e.g., zeolites or MOFs, typically show a much weaker adsorption of cycloalkanes.[28c,e,32d,36] Adsorption enthalpies of C_5-C_8 cycloalkanes are up to −17 kJ/mol lower than those of the corresponding linear chains (Figure 8, Table S2). This allows the chromatographic separation of cyclic hydrocarbons from linear ones, with the unusual preference for selectively adsorbing the cyclic molecule, as illustrated in the chromatograms in Figure 1 where cyclohexane elutes much later than *n*-octane. *n*-Octane has two carbon atoms more but a lower retention time. Henry constants are 2−14 times larger for cycloalkanes compared to *n*-alkanes (Table 4). The selectivity varies significantly among the different UiO-66 forms. For the selected case of cycloheptane−*n*-heptane, the ratio of Henry constants is 9.5 for UiO-66, 13.0 for UiO-66-Me, 4.3 for UiO-66-NO_2, and 5.5 for UiO-66-Me_2. A size effect in this separation of linear and cyclic molecules was observed. The difference in adsorption enthalpy, pre-exponential factor, and Henry constant between linear and cyclic molecules first increases with carbon number, and then again decreases from C_8 on (Figure 8, Table S1).

An explanation of these observations can be found in the shape and size fitting between the cycloalkanes and the UiO-66 cages. At a size of about eight CH_2 groups, the smallest cage of UiO-66 is optimally filled (vide supra), thus increasing the enthalpic interaction. Moreover, the better fit of these cycloalkanes within the UiO-66 cages results in a larger overall freedom to reorientate as compared to the linear chains, giving an entropic advantage. The largest dimension of these molecules is roughly of the same size as the inner pore diameter of the smallest, tetrahedral cage in the framework. For even larger *n*-alkanes (carbon number of 10 or higher), preferential adsorption of cycloalkanes over linear alkanes is no longer observed. This molecular sitting was further investigated using Monte Carlo simulations.

3.1.3. Stereoisomer Adsorption and Separation. The commensurate fitting of cyclic molecules in the UiO-66 structure gives rise to a very sensitive and discriminative

Table 4. Experimental Adsorption Selectivity of Cyclic over Linear Alkanes on UiO-66, UiO-66-Me, UiO-66-NO_2, and UiO-66-Me_2 at 523 K, Calculated As the Ratio of Henry Constants at 523 K

N_c[a]	UiO-66[b]	UiO-66-Me[b]	UiO-66-NO_2[b]	UiO-66-Me_2[b]
5	1.9	2.3		2.2
6	5.7	6.1	4.4	3.7
7	9.5	13.0	4.3	5.5
8	14.4	14.0	6.2	5.8
10		2.6		2.1
12	2.4			

[a]Number of carbon atoms. [b]Selectivity cyclic/linear alkanes at 523 K.

dx.doi.org/10.1021/jp402294h | J. Phys. Chem. C 2013, 117, 12567−12578

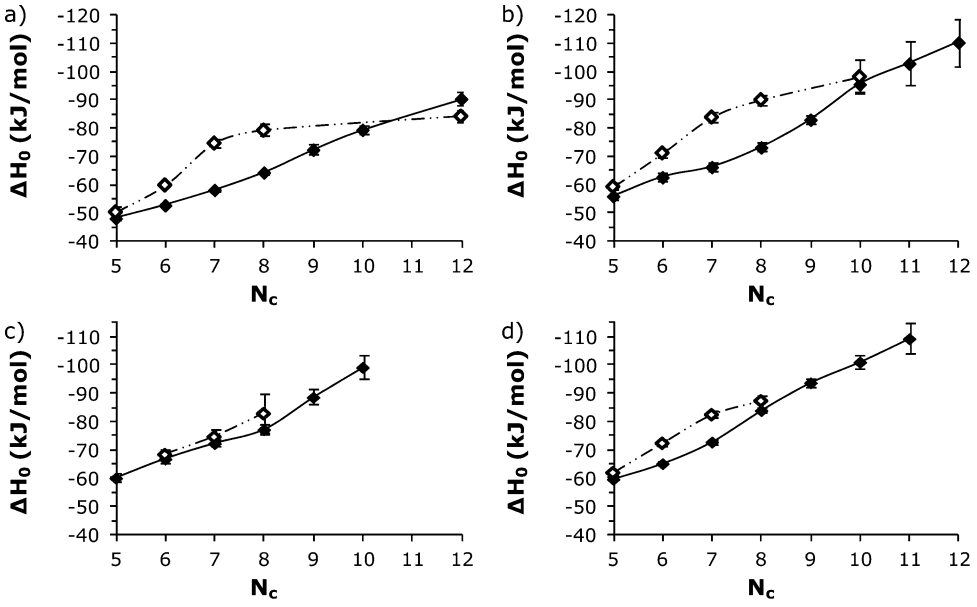

Figure 8. Experimental adsorption enthalpy as a function of carbon number N_c for linear (♦) and cyclic alkanes (◊) on UiO-66 (a), UiO-66-Me (b), UiO-66-NO_2 (c) and UiO-66-Me_2 (d).

relationship between molecular structure and adsorption properties, which can be exploited to separate molecules with nearly identical physicochemical properties. Using the confinement resulting from the UiO-66 framework, the separation of cis- and trans-isomer of 1,2-, 1,3-, or 1,4-dimethylcyclohexanes is achieved (Figure 9). These materials allow for shape selective separation, discriminating on position and orientation (axial or equatorial) of the substituent. In all cases, the stereoisomer with both substituents (*trans*-1,2, *cis*-1,3, or *trans*-1,4) in equatorial position is less strongly adsorbed. The separation factor is function of the organic linker in the framework. The unfunctionalized material UiO-66 separated the 1,4-dimethylcyclohexane isomers more efficiently (α = 2.1) than 1,2- and 1,3-dimethylcyclohexane isomers (α = 1.7−1.8). The UiO-66-Me material has a similar performance for each couple of isomers (α = 2.0−2.1). A lower adsorption selectivity (α = 1.5−1.7) is observed for UiO-66-NO_2 and UiO-66-Me_2. Generally, the difference in adsorption enthalpy between cis/trans isomers amounts to 4−6 kJ/mol. In the compensation plot between adsorption enthalpy and pre-exponential entropic factors (Figure 10), two distinct clusters of isomers are observed,

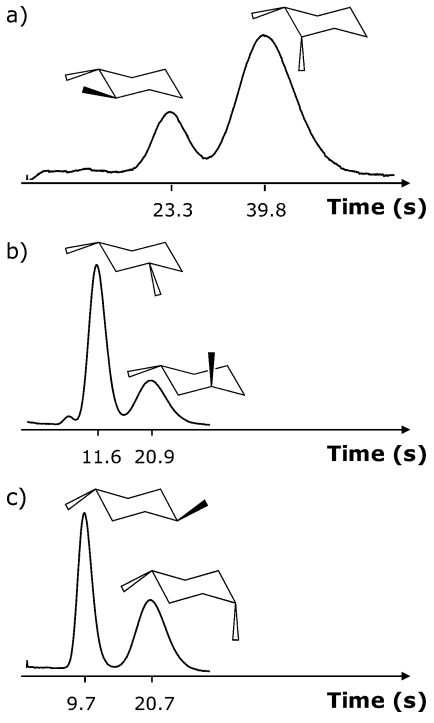

Figure 9. (a−c) Chromatographic profiles of 1,2-, 1,3-, and 1,4-dimethylcyclohexanes on UiO-66 at 373 K; isomers are structurally depicted next to the respective peaks.

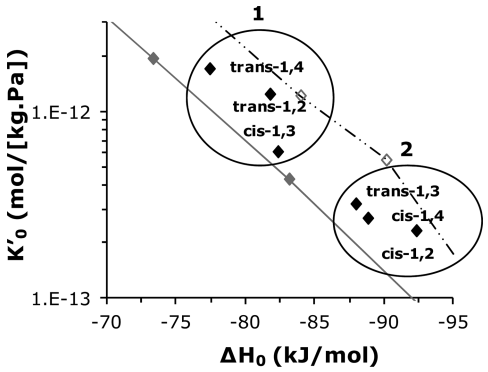

Figure 10. Experimental adsorption enthalpies and pre-exponential factors (adsorption entropy) of dimethylcyclohexane isomers (♦) on UiO-66-Me. Linear alkanes (♦, full line) and cycloalkanes (◊, dashed line) are also shown.

grouping isomers with both substituents equatorially oriented on the one hand (1) and isomers with one substituent axially and the other one equatorial oriented on the other hand (2). The resulting molecular shape is more ellipsoidal in the first case and more spherical in the latter case. This spherical shape results in a significantly larger adsorption enthalpy. A more in-depth analysis and the possible influence of entropic factors were done using Monte Carlo simulations.

dx.doi.org/10.1021/jp402294h | J. Phys. Chem. C 2013, 117, 12567−12578

The separation properties for dimethylcyclohexane cis- and trans-isomers are extendable to other molecules, as illustrated for cis- and trans-isomers within 2-hexene or 3-hexene (Figure 11). The 1-hexene coincides with *cis*-3-hexene. Chromatograms

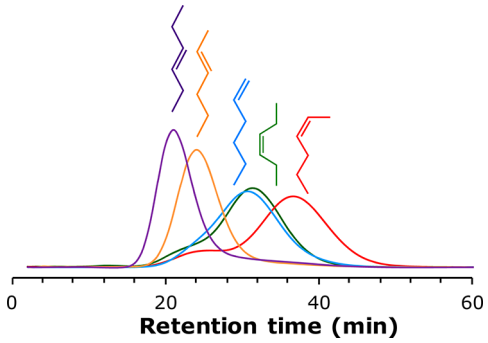

Figure 11. Separation of *cis*- and *trans*-alkenes on UiO-66 on UiO-66, UiO-66-Me, and UiO-66-NO_2 at 523 K.

were recorded by injection of pure compounds, and an overlay was made afterward. Limited isomerization to *trans*-2-hexene seems to occur and most likely occurs at the open metal sites, resulting from missing liners in the framework.[37] Distinction between *cis*-2-heptene and *trans*-3-heptene was achieved as well but proved to be less efficient. The latter indicates a size effect and points toward the tetrahedral cage as the selective site.

3.2. Monte Carlo Simulations. In order to further study the experimentally observed size and selectivity effects in the adsorption of linear and cyclic alkanes, a Monte Carlo simulation study was performed. This study is limited to the unfunctionalized UiO-66. Initial parameters to describe the framework properties were taken from the UFF and Dreiding.[30] These parameters were previously used by Wiersum et al. in a study on CO_2 and CH_4 storage in UiO-66.[18d] The structures and parameters for *n*-alkanes were taken from the TraPPE set and extended to cyclic alkanes based on published molecular structures.[38] In general, both force fields describe the trend in adsorption enthalpy quite well (Table S3, Figure S7) and yield similar results. The UFF parameters results in closer adsorption enthalpy predictions for C_{8-11} and equally good results for adsorption entropy than the Dreiding parameters (Figure S7–S8, Table S3). The comparison between both force fields was done without any Lennard–Jones parameter strength tuning. The number of cycles was optimized to limit the respective error margins to <1%. A lower number of cycles was needed for UFF. On the basis of these observations, UFF was used in other Monte Carlo simulations.

In the simulations, a significant entropy gain of ca. 20–25 J/[mol·K] for C_5–C_{10} for cyclic molecules was observed compared to their linear counterparts besides an increased enthalpic interaction. Starting from *n*-octane, the simulated entropy values agree well with the experimental trend (Figure S8). The simulated adsorption enthalpy increases between ethane and dodecane. A good agreement in enthalpy values was found between simulated (−57.3, −56.1 kJ/mol) and experimental data (−54.8 kJ/mol) for *n*-pentane (lowest experimental value). Between *n*-hexane and *n*-octane, the adsorption enthalpy varies only a little with increasing carbon number (Figure S7). This indicates occurrence of cage/windows effects: the adsorbate experiences an energy barrier to enter a cage through the window or preferentially sits in either the small or large cage of the framework. The temperature effect on adsorption properties was investigated for linear alkanes in the range of 100–600 K. In the studied temperature range, the adsorption enthalpy has little influence on the smaller ($\leq C_5$) and largest ($\geq C_{10}$) *n*-alkanes besides the C_6–C_9 range. Here, a much larger spreading (10–20 kJ/mol) is observed. This is consistent with the previously mentioned window/cage effect. At 100 K, the trend of simulated adsorption enthalpy with carbon number no longer follows the general trend as obtained at higher temperatures (Figure 12). At low temperatures, the estimation of adsorbate–

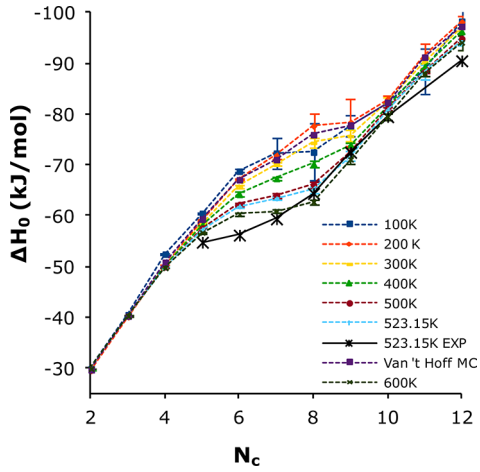

Figure 12. Simulated temperature dependence of adsorption enthalpy for C_2–C_{12} *n*-alkanes using Monte Carlo (UFF force field, errors <1%).

adsorbent interaction energies is no longer accurate (increasing errors, loss of systematic trend), even at relatively high numbers of computational cycles (up to 4 000 000). The bad performance at very low temperatures could be expected, as classical force fields are developed to describe the liquid/vapor phase equilibrium while the studied adsorbates are solid in these conditions.

3.2.1. Molecular Sitting. The above-discussed indications of a significant cage/size effect between C_6–C_9 (Figures 12 and S7). This corresponds to the zone where the size of the molecule, in unfolded or partly folded conformation, approaches the size of the tetrahedral cage. In order to verify this hypothesis, additional simulations were performed to verify the actual position of 1 molecule over 100 000 Monte Carlo cycles. Either by visual inspection of the simulation box or plotting the adsorbates' mass density points, the molecular position can be verified. To give an overview, a small (*n*-butane), intermediate (*n*-octane), and large (*n*-dodecane) *n*-alkane was selected. The density plots show dense clustering at distinct positions for *n*-butane and *n*-dodecane, respectively, in the tetrahedral (small) and octahedral (large) cages (Figure 13). A distribution between both cages is found for *n*-octane. The latter is the effect of different molecular conformations or "folding" that *n*-octane adopts. In a denser state (folded), the overall size fits nicely in the smaller cage. When unfolded, the alkyl chain is curved onto the wall of the octahedral wall, as follows from visual inspection of the simulation box.

Figure 14 shows a comparative graph of simulated (◊) and experimental (♦) adsorption enthalpy for cycloalkanes. Compared to linear molecules, a larger deviation can be noticed between experiment and simulation (Tables S2–S3).

dx.doi.org/10.1021/jp402294h | J. Phys. Chem. C 2013, 117, 12567–12578

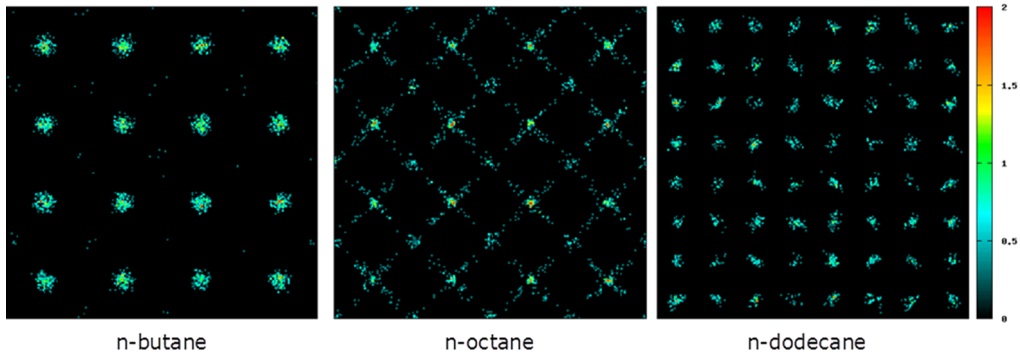

Figure 13. Density plots showing the "center of gravity" of *n*-butane, *n*-octane, and *n*-dodecane projected on the *XY* plane of the UiO-66 Monte Carlo simulation box (2 × 2 × 2 unit cells). Left: the small cages are populated by *n*-butane. The dense cluster coincides with the position of the small cage. Middle: *n*-octane is proportionally distributed between the small and large cage. Right: the center of mass of *n*-dodecane is exclusively plotted in the large cage, but the size of the molecule requires partial sitting of the small cage as well.

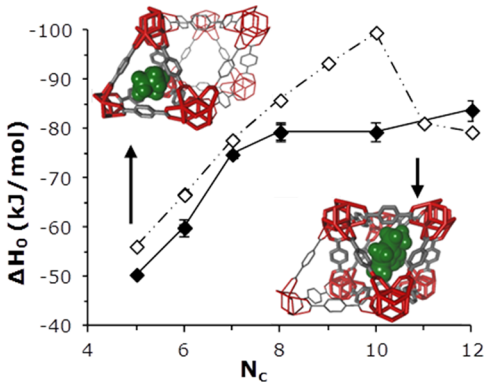

Figure 14. Experimental (♦) and simulated (◊) adsorption energies of cycloalkanes on UiO-66. The insets in the graph show the positioning of cyclopentane in the small cage and cycloundecane in the large cage. The steep step at cycloundecane in the simulations is explained by the exclusive positioning of the largest molecules in the largest cages during simulations at zero coverage.

This is likely because the isomers were modeled as rigid units (computational limitation). With increasing molecular size, the prediction overestimates the adsorption enthalpy more but still follows the general trend. At cycloundecane, a switch in molecular positioning is found. In the simulation, the preferential adsorption site is now the larger, octahedral cage and no longer the smallest, tetrahedral cage. The experimental tendency of adsorption enthalpy with carbon number indicates that a more gradual switch in preferential adsorption site is likely than predicted by simulations. Molecular position and cage sites are depicted in Figure S10.

3.2.2. Stereoisomer Separation. To gain a better insight in the mechanism governing the stereoisomers' separation, adsorption of the different dimethylcyclohexanes was simulated at zero coverage. The simulations confirm the trends observed in the experimental data: limited differences in enthalpic and entropic factors. The simulated data attribute a higher weight to entropic factors than the experimental data do. The differences in enthalpic factors are lower: 1−3 kJ/mol compared to 3−4 kJ/mol. On the basis of the ratio of calculated Henry constants, an estimate for experimental selectivity is made. In Table 5, the proportion of Henry coefficients at 523 K for cis/trans isomers is given. Preferential adsorption selectivity as determined by inverse pulse gas chromatography was reproduced: isomers with both methyl groups in equatorial position (trans) are less retained. As in the previous paragraph, one molecule NVT simulations were performed to investigate the preferential adsorption site. All isomers preferentially sit in the tetrahedral cage.

Table 5. Simulated and Experimental Adsorption Selectivity, Calculated As the Ratio of Henry Constants of Cis and Trans Isomer at Zero Coverage, on UiO-66 at 523 K

molecule	experimental	simulation
1,2-dimethylcyclohexane	1.7	3.0
1,3-dimethylcyclohexane	0.6	0.2
1,4-dimethylcyclohexane	2.1	3.9

4. CONCLUSION

The inverse pulse chromatographic data show the potential of tuning adsorption strength and selectivity by introducing functional groups in the pores by modified organic linkers. Our study shows that differences between UiO-66 materials largely result from reduction in effective pore size by functional groups rather than by the polar character of the organic linkers (e.g., UiO-66-NO_2). A strong size dependency of adsorption properties was observed, depending on the nature of the molecule. Monte Carlo simulations showed that size and shape selectivity results from an optimal fitting in the small tetrahedral cage of the UiO-66 framework. This results in a nonlinear increase in adsorption strength for *n*-alkanes and a pronounced preference for adsorbing cyclic molecules, as such molecules are commensurate to the shape of these cages. By means of resulting confinement, stereoisomers can be separated on UiO-66 materials. We successfully demonstrated this for cis/trans alkenes and dimethylcyclohexanes. Exploitation of this confinement effect at higher loading or in liquid phase is of interest for future work.

■ ASSOCIATED CONTENT

Ⓢ Supporting Information

Complementary material in the form of graphs and tables. This material is available free of charge via the Internet at http://pubs.acs.org.

■ AUTHOR INFORMATION

Corresponding Author

*E-mail: joeri.denayer@vub.ac.be.

Notes

The authors declare no competing financial interest.

■ ACKNOWLEDGMENTS

S.C. thanks ERC-StG'11 (RASPA Project) and MICINN (CTQ2010-16077/BQU project). J.D. and D.D.V. are grateful to FWO Vlaanderen for financial support (G.0453.09 N). T.D. acknowledges FWO Vlaanderen for his research visit (V.4157.12.N).

■ REFERENCES

(1) (a) Czaja, A. U.; Trukhan, N.; Muller, U. Industrial Applications of Metal-Organic Frameworks. *Chem. Soc. Rev.* **2009**, *38* (5), 1284−1293. (b) Huang, H.-J.; Ramaswamy, S.; Tschirner, U. W.; Ramarao, B. V. A Review of Separation Technologies in Current and Future Biorefineries. *Sep. Purif. Technol.* **2008**, *62* (1), 1−21. (c) Meek, S. T.; Greathouse, J. A.; Allendorf, M. D. Metal-Organic Frameworks: A Rapidly Growing Class of Versatile Nanoporous Materials. *Adv. Mater.* **2011**, *23* (2), 249−267.

(2) Atkinson, B. *Cyclohexyl Amide Derivates as CRF Receptor Anatgonists*. U.S. Patent 20110128, 2011.

(3) Erman Mark, B., W. P. J. *Physiological Cooling Compositions Containing Highly Purified Ethylester of N-[[5-methyl-2-(1-methylethyl) cyclohexyl] Carbonyl]glycine*, WO Patent 2005097735 A1, 2007.

(4) Akiyama, A. *Purification Methods of Liquid Crystal Compounds and Liquid Crystal Composition*. EP 0603731 B1, 2005.

(5) (a) Gasparrini, F.; Misiti, D.; Villani, C. High-Performance Liquid Chromatography Chiral Stationary Phases Based on Low-Molecular-Mass Selectors. *J. Chromatogr., A* **2001**, *906* (1−2), 35−50. (b) Maier, N. M.; Franco, P.; Lindner, W. Separation of Enantiomers: Needs, Challenges, Perspectives. *J. Chromatogr., A* **2001**, *906* (1−2), 3−33.

(6) (a) Stock, N.; Biswas, S. Synthesis of Metal-Organic Frameworks (MOFs): Routes to Various MOF Topologies, Morphologies, and Composites. *Chem. Rev.* **2011**, *112* (2), 933−969. (b) Li, J.-R.; Sculley, J.; Zhou, H.-C. Metal-Organic Frameworks for Separations. *Chem. Rev.* **2012**, *112* (2), 869−932. (c) Jiang, H.-L.; Xu, Q. Porous Metal-Organic Frameworks as Platforms for Functional Applications. *Chem. Commun.* **2011**, *47* (12), 3351−3370.

(7) (a) Li, J.-R.; Sculley, J.; Zhou, H.-C. Metal−Organic Frameworks for Separations. *Chem. Rev.* **2011**, *112* (2), 869−932. (b) Wu, H.; Gong, Q.; Olson, D. H.; Li, J. Commensurate Adsorption of Hydrocarbons and Alcohols in Microporous Metal Organic Frameworks. *Chem. Rev.* **2012**, *112* (2), 836−868.

(8) (a) Li, J.-R.; Kuppler, R. J.; Zhou, H.-C. Selective Gas Adsorption and Separation in Metal-Organic Frameworks. *Chem. Soc. Rev.* **2009**, *38* (5), 1477−1504. (b) Nickerl, G.; Henschel, A.; Grünker, R.; Gedrich, K.; Kaskel, S. Chiral Metal-Organic Frameworks and Their Application in Asymmetric Catalysis and Stereoselective Separation. *Chem. Ing. Tech.* **2011**, *83* (1−2), 90−103.

(9) (a) Watanabe, T.; Sholl, D. S. Accelerating Applications of Metal-Organic Frameworks for Gas Adsorption and Separation by Computational Screening of Materials. *Langmuir* **2012**, *28* (40), 14114−14128. (b) Bao, X.; Broadbelt, L. J.; Snurr, R. Q. Computational Screening of Homochiral Metal-Organic Frameworks for Enantioselective Adsorption. *Microporous Mesoporous Mater.* **2012**, *157*, 118−123. (c) Greathouse, J. A.; Ockwig, N. W.; Criscenti, L. J.; Guilinger, T. R.; Pohl, P.; Allendorf, M. D. Computational Screening of Metal-Organic Frameworks for Large-Molecule Chemical Sensing. *Phys. Chem. Chem. Phys.* **2010**, *12* (39), 12621−12629. (d) Wilmer, C. E.; Leaf, M.; Lee, C. Y.; Farha, O. K.; Hauser, B. G.; Hupp, J. T.; Snurr, R. Q. Large-Scale Screening of Hypothetical Metal-Organic Frameworks. *Nat. Chem.* **2012**, *4* (2), 83−89.

(10) (a) Dybtsev, D. N.; Yutkin, M. P.; Peresypkina, E. V.; Virovets, A. V.; Serre, C.; Ferey, G.; Fedin, V. P. Isoreticular Homochiral Porous Metal-Organic Structures with Tunable Pore Sizes. *Inorg. Chem.* **2007**, *46* (17), 6843−6845. (b) Nuzhdin, A. L.; Dybtsev, D. N.; Bryliakov, K. P.; Talsi, E. P.; Fedin, V. P. Enantioselective Chromatographic Resolution and One-Pot Synthesis of Enantiomerically Pure Sulfoxides over a Homochiral Zn-Organic Framework. *J. Am. Chem. Soc.* **2007**, *129* (43), 12958−+. (c) Suh, K.; Yutkin, M. P.; Dybtsev, D. N.; Fedin, V. P.; Kim, K. Enantioselective Sorption of Alcohols in a Homochiral Metal-Organic Framework. *Chem. Commun.* **2012**, *48* (4), 513−515. (d) Yutkin, M. P.; Dybtsev, D. N.; Fedin, V. P. Homochiral Porous Metal-Organic Coordination Polymers: Synthesis, Structure and Functional Properties. *Russ. Chem. Rev.* **2011**, *80* (11), 1009−1034.

(11) Cavka, J. H.; Jakobsen, S.; Olsbye, U.; Guillou, N.; Lamberti, C.; Bordiga, S.; Lillerud, K. P. A new Zirconium Inorganic Building Brick Forming Metal Organic Frameworks with Exceptional Stability. *J. Am. Chem. Soc.* **2008**, *130* (42), 13850−13851.

(12) (a) Garibay, S. J.; Cohen, S. M. Isoreticular Synthesis and Modification of Frameworks with the UiO-66 Topology. *Chem. Commun.* **2010**, *46* (41), 7700−7702. (b) Foo, M. L.; Horike, S.; Fukushima, T.; Hijikata, Y.; Kubota, Y.; Takata, M.; Kitagawa, S. Ligand-Based Solid Solution Approach to Stabilisation of Sulphonic Acid Groups in Porous Coordination Polymer Zr6O4(OH)(4)(BDC)(6) (UiO-66). *Dalton Trans.* **2012**, *41* (45), 13791−13794. (c) Kim, M.; Cahill, J. F.; Fei, H.; Prather, K. A.; Cohen, S. M. Postsynthetic Ligand and Cation Exchange in Robust Metal-Organic Frameworks. *J. Am. Chem. Soc.* **2012**, *134* (43), 18082−18088. (d) Kim, M.; Cahill, J. F.; Su, Y.; Prather, K. A.; Cohen, S. M. Postsynthetic Ligand Exchange as a Route to Functionalization of 'Inert' Metal-Organic Frameworks. *Chem. Sci.* **2012**, *3* (1), 126−130. (e) Abid, H. R.; Ang, H. M.; Wang, S. Effects of Ammonium Hydroxide on the Structure and Gas Adsorption of Nanosized Zr-MOFs (UiO-66). *Nanoscale* **2012**, *4* (10), 3089−3094. (f) Morris, W.; Doonan, C. J.; Yaghi, O. M. Postsynthetic Modification of a Metal-Organic Framework for Stabilization of a Hemiaminal and Ammonia Uptake. *Inorg. Chem.* **2011**, *50* (15), 6853−6855. (g) Zlotea, C.; Phanon, D.; Mazaj, M.; Heurtaux, D.; Guillerm, V.; Serre, C.; Horcajada, P.; Devic, T.; Magnier, E.; Cuevas, F.; Ferey, G.; Llewellyn, P. L.; Latroche, M. Effect of NH2 and CF3 Functionalization on the Hydrogen Sorption Properties of MOFs. *Dalton Trans.* **2011**, *40* (18), 4879−4881. (h) Kandiah, M.; Nilsen, M. H.; Usseglio, S.; Jakobsen, S.; Olsbye, U.; Tilset, M.; Larabi, C.; Quadrelli, E. A.; Bonino, F.; Lillerud, K. P. Synthesis and Stability of Tagged UiO-66 Zr-MOFs. *Chem. Mater.* **2010**, *22* (24), 6632−6640.

(13) Schaate, A.; Roy, P.; Godt, A.; Lippke, J.; Waltz, F.; Wiebcke, M.; Behrens, P. Modulated Synthesis of Zr-Based Metal-Organic Frameworks: From Nano to Single Crystals. *Chem.—Eur. J.* **2011**, *17* (24), 6643−6651.

(14) (a) Jasuja, H.; Zang, J.; Sholl, D. S.; Walton, K. S. Rational Tuning of Water Vapor and CO2 Adsorption in Highly Stable Zr-Based MOFs. *J. Phys. Chem. C* **2012**, *116* (44), 23526−23532. (b) Schoenecker, P. M.; Carson, C. G.; Jasuja, H.; Flemming, C. J.; Walton, K. S. Effect of Water Adsorption on Retention of Structure and Surface Area of Metal-Organic Frameworks. *Ind. Eng. Chem. Res.* **2012**, *51* (18), 6513−6519.

(15) (a) Vermoortele, F.; Vandichel, M.; Van de Voorde, B.; Ameloot, R.; Waroquier, M.; Van Speybroeck, V.; De Vos, D. E. Electronic Effects of Linker Substitution on Lewis Acid Catalysis with Metal-Organic Frameworks. *Angew. Chem., Int. Ed.* **2012**, *51* (20), 4887−4890. (b) Vermoortele, F.; Ameloot, R.; Vimont, A.; Serre, C.; De Vos, D. An Amino-Modified Zr-terephthalate Metal-Organic Framework as an Acid-Base Catalyst for Cross-aldol Condensation. *Chem. Commun.* **2011**, *47* (5), 1521−1523.

(16) (a) Valenzano, L.; Civalleri, B.; Chavan, S.; Bordiga, S.; Nilsen, M. H.; Jakobsen, S.; Lillerud, K. P.; Lamberti, C. Disclosing the Complex Structure of UiO-66 Metal Organic Framework: A Synergic Combination of Experiment and Theory. *Chem. Mater.* **2011**, *23* (7), 1700−1718. (b) Devautour-Vinot, S.; Maurin, G.; Serre, C.; Horcajada, P.; da Cunha, D. P.; Guillerm, V.; Costa, E. d. S.; Taulelle, F.; Martineau, C. Structure and Dynamics of the Functionalized MOF Type UiO-66(Zr): NMR and Dielectric Relaxation Spectroscopies Coupled with DFT Calculations. *Chem. Mater.* **2012**, *24* (11), 2168−2177.

(17) Kolokolov, D. I.; Stepanov, A.; Guillerm, V.; Serre, C.; Frick, B.; Jobic, H. Probing the Dynamics of the Porous Zr Terephthalate UiO-

66 Framework Using H-2 NMR and Neutron Scattering. *J. Phys. Chem. C* **2012**, *116* (22), 12131−12136.
(18) (a) Yang, Q.; Guillerm, V.; Ragon, F.; Wiersum, A. D.; Llewellyn, P. L.; Zhong, C.; Devic, T.; Serre, C.; Maurin, G. CH_4 storage and CO_2 Capture in Highly Porous Zirconium Oxide Based Metal-Organic Frameworks. *Chem. Commun.* **2012**, *48* (79), 9831−9833. (b) Abid, H. R.; Tian, H.; Ang, H. M.; Tade, M. O.; Buckley, C. E.; Wang, S. Nanosize Zr-Metal Organic Framework (UiO-66) for Hydrogen and Carbon Dioxide Storage. *Chem Eng. J.* **2012**, *187*, 415−420. (c) Chavan, S.; Vitillo, J. G.; Gianolio, D.; Zavorotynska, O.; Civalleri, B.; Jakobsen, S.; Nilsen, M. H.; Valenzano, L.; Lamberti, C.; Lillerud, K. P.; Bordiga, S. H-2 Storage in Isostructural UiO-67 and UiO-66 MOFs. *Phys. Chem. Chem. Phys.* **2012**, *14* (5), 1614−1626. (d) Wiersum, A. D.; Soubeyrand-Lenoir, E.; Yang, Q.; Moulin, B.; Guillerm, V.; Ben Yahia, M.; Bourrelly, S.; Vimont, A.; Miller, S.; Vagner, C.; Daturi, M.; Clet, G.; Serre, C.; Maurin, G.; Llewellyn, P. L. An Evaluation of UiO-66 for Gas-Based Applications. *Chem.—Asian J.* **2011**, *6* (12), 3270−3280. (e) Yang, Q.; Jobic, H.; Salles, F.; Kolokolov, D.; Guillerm, V.; Serre, C.; Maurin, G. Probing the Dynamics of CO2 and CH4 within the Porous Zirconium Terephthalate UiO-66(Zr): A Synergic Combination of Neutron Scattering Measurements and Molecular Simulations. *Chem.—Eur. J.* **2011**, *17* (32), 8882−8889. (f) Yang, Q.; Wiersum, A. D.; Llewellyn, P. L.; Guillerm, V.; Serred, C.; Maurin, G. Functionalizing Porous Zirconium Terephthalate UiO-66(Zr) for Natural Gas Upgrading: a Computational Exploration. *Chem. Commun.* **2011**, *47* (34), 9603−9605.
(19) Soubeyrand-Lenoir, E.; Vagner, C.; Yoon, J. W.; Bazin, P.; Ragon, F.; Hwang, Y. K.; Serre, C.; Chang, J. S.; Llewellyn, P. L. How Water Fosters a Remarkable 5-Fold Increase in Low-Pressure CO_2 Uptake within Mesoporous MIL-100(Fe). *J. Am. Chem. Soc.* **2012**, *134* (24), 10174−10181.
(20) Nik, O. G.; Chen, X. Y.; Kaliaguine, S. Functionalized Metal Organic Framework-Polyimide Mixed Matrix Membranes for CO_2/CH_4 Separation. *J. Membr. Sci.* **2012**, *413*, 48−61.
(21) Huang, Y.; Qin, W.; Li, Z.; Li, Y. Enhanced Stability and CO_2 Affinity of a UiO-66 type Metal-Organic Framework Decorated with Dimethyl Groups. *Dalton Trans.* **2012**, *41* (31), 9283−9285.
(22) (a) Barcia, P. S.; Guimaraes, D.; Mendes, P. A.; Silva, J. A.; Guillerm, V.; Chevreau, H.; Serre, C.; Rodrigues, A. E. Reverse Shape Selectivity in the Adsorption of Hexane and Xylene Isomers in MOF UiO-66. *Microporous Mesoporous Mater.* **2011**, *139* (1−3), 67−73. (b) Moreira, M. A.; Santos, J. C.; Ferreira, A. F.; Loureiro, J. M.; Ragon, F.; Horcajada, P.; Shim, K. E.; Hwang, Y. K.; Lee, U.; Chang, J. S.; Serre, C.; Rodrigues, A. E. Reverse Shape Sellectivity in the Liquid-Phase Adsorption of Xylene Isomers in Zirconium Terephthalate MOF UiO-66. *Langmuir* **2012**, *28* (13), 5715−5723.
(23) Chang, N.; Yan, X. P. Exploring Reverse Shape Selectivity and Molecular Sieving Effect of Metal-Organic Framework UIO-66 Coated Capillary Column for Gas Chromatographic Separation. *J. Chromatogr., A* **2012**, *1257*, 116−124.
(24) (a) Denayer, J. F. M.; Baron, G. V. The Confinement Factor: A Thermodynamic Parameter to Characterize Microporous Adsorbents. *Adsorpt.-J. Int. Adsorpt. Soc.* **2005**, *11*, 85−90. (b) Chen, C. Y.; Zones, S. I. Characterization of Zeolites via Vapor Phase Physisorption of Hydrocarbons. *Microporous Mesoporous Mater.* **2007**, *104* (1−3), 39−45.
(25) (a) Eder, F.; Stockenhuber, M.; Lercher, J. A. *Sorption of Light Alkanes on H-ZSM5 and H-Mordenite*; Elsevier Science Publ B V: Amsterdam, 1995; Vol. *97*, pp 495−500; (b) Arik, I. C.; Denayer, J. F.; Baron, G. V. High-Temperature Adsorption of *n*-Alkanes on ZSM-5 Zeolites: Influence of the Si/Al Ratio and the Synthesis Method on the Low-Coverage Adsorption Properties. *Microporous Mesoporous Mater.* **2003**, *60* (1−3), 111−124. (c) Denayer, J. F.; Baron, G. V.; Martens, J. A.; Jacobs, P. A. Chromatographic Study of Adsorption of *n*-Alkanes on Zeolites at High Temperatures. *J. Phys. Chem. B* **1998**, *102* (17), 3077−3081. (d) Denayer, J. F. M.; Baron, G. V. Adsorption of Normal and Branched Paraffins in Faujasite Zeolites NaY, HY, Pt/NaY and USY. *Adsorption-J. Int. Adsorpt. Soc,* **1997**, 3 (4), 251−265. (e) Denayer, J. F. M.; Ocakoglu, R. A.; Thybaut, J.; Marin, G.; Jacobs, P.; Martens, J.; Baron, G. V. n- and Isoalkane Adsorption Mechanisms on Zeolite MCM-22. *J. Phys. Chem. B* **2006**, *110* (17), 8551−8558.
(26) (a) Duerinck, T.; Leflaive, P.; Arik, I. C.; Pirngruber, G.; Meynen, V.; Cool, P.; Martens, J. A.; Baron, G. V.; Faraj, A.; Denayer, J. F. M. Experimental and Statistical Modeling Study of Low Coverage Gas Adsorption of Light Alkanes on Meso-Microporous Silica. *Chem. Eng. J.* **2012**, *179* (0), 52−62. (b) Devriese, L. â. I.; Cools, L.; Aerts, A.; Martens, J. â. A.; Baron, G. â. V.; Denayer, J. â. F. Shape Selectivity in Adsorption of n- and Iso-alkanes on a Zeotile-2 Microporous/Mesoporous Hybrid and Mesoporous MCM-48. *Adv. Funct. Mater.* **2007**, *17* (18), 3911−3917. (c) Devriese, L. I.; Cools, L.; Aerts, A.; Martens, J. A.; Baron, G. V.; Denayer, J. F. M. Shape Selectivity in Adsorption of Microporous/Mesoporous Hybrid n- and iso-Alkanes on a Zeotile-2 and Mesoporous MCM-48. *Adv. Funct. Mater.* **2007**, *17* (18), 3911−3917. (d) Vartuli, J. C.; Malek, A.; Roth, W. J.; Kresge, C. T.; McCullen, S. B. The Sorption Properties of as-Synthesized and Calcined MCM-41 and MCM-48. *Microporous Mesoporous Mater.* **2001**, *44*−*45*, 691−695. (e) Eder, F.; He, Y. J.; Nivarthy, G.; Lercher, J. A. Sorption of Alkanes on Novel Pillared Zeolites; Comparison between MCM-22 and MCM-36. *Recl. Trav. Chim. Pays-Bas-J. R. Neth. Chem. Soc.* **1996**, *115* (11−12), 531−.
(27) (a) Lopezgarzon, F. J.; Pyda, M.; Domingogarcia, M. Studies of the Surface-Properties of Active Carbons by Iinverse Gas-Chromatography at Infinite Dilution. *Langmuir* **1993**, *9* (2), 531−536. (b) Jagiello, J.; Bandosz, T. J.; Schwarz, J. A. Study of Carbon Microstructure by Using Inverse Gas-Chromatography. *Carbon* **1994**, *32* (4), 687−691.
(28) (a) Finsy, V.; De Bruyne, S.; Alaerts, L.; De Vos, D.; Jacobs, P. A.; Baron, G. V.; Denayer, J. F. M., Shape Selective Adsorption of Linear and Branched Alkanes in the Cu(3)(BTC)(2) Metal-Organic Framework. In *From Zeolites to Porous Mof Materials: The 40th Anniversary of International Zeolite Conference, Proceedings of the 15th International Zeolite Conference*; Xu, R.; Gao, Z.; Chen, J.; Yan, W., Eds.; Elsevier Science: Amsterdam, 2007; Vol. *170*, pp 2048−2053. (b) Maes, M.; Alaerts, L.; Vermoortele, F.; Ameloot, R.; Couck, S.; Finsy, V.; Denayer, J. F. M.; De Vos, D. E. Separation of C-5-Hydrocarbons on Microporous Materials: Complementary Performance of MOFs and Zeolites. *J. Am. Chem. Soc.* **2010**, *132* (7), 2284−2292. (c) Couck, S.; Remy, T.; Baron, G. V.; Gascon, J.; Kapteijn, F.; Denayer, J. F. M. A Pulse Chromatographic Study of the Adsorption Properties of the Amino-MIL-53 (Al) Metal-Organic Framework. *Phys. Chem. Chem. Phys.* **2010**, *12* (32), 9413−9418. (d) Duerinck, T.; Couck, S.; Vermoortele, F.; De Vos, D. E.; Baron, G. V.; Denayer, J. F. M. Pulse Gas Chromatographic Study of Adsorption of Substituted Aromatics and Heterocyclic Molecules on MIL-47 at Zero Coverage. *Langmuir* **2012**, *28* (39), 13883−13891. (e) Finsy, V.; Calero, S.; Garcia-Perez, E.; Merkling, P. J.; Vedts, G.; De Vos, D. E.; Baron, G. V.; Denayer, J. F. M. Low-Coverage Adsorption Properties of the Metal-Organic Framework MIL-47 Studied by Pulse Chromatography and Monte Carlo Simulations. *Phys. Chem. Chem. Phys.* **2009**, *11* (18), 3515−3521.
(29) Ocakoglu, R. A.; Denayer, J. F. M.; Marin, G. B.; Martens, J. A.; Baron, G. V. Tracer Chromatographic Study of Pore and Pore Mouth Adsorption of Linear and Monobranched Alkanes on ZSM-22 Zeolite. *J. Phys. Chem. B* **2002**, *107* (1), 398−406.
(30) (a) Rappe, A. K.; Casewit, C. J.; Colwell, K. S.; Goddard, W. A.; Skiff, W. M. UFF, a Full Periodic-Table Force-Field For Molecular Mechanics and Molecular-Dynamics Simulations. *J. Am. Chem. Soc.* **1992**, *114* (25), 10024−10035. (b) Mayo, S. L.; Olafson, B. D.; Goddard, W. A. Dreiding - A Generic Force-Field for Molecular Simulations. *J. Phys. Chem.* **1990**, *94* (26), 8897−8909.
(31) Schenk, M.; Smit, B.; Maesen, T. L. M.; Vlugt, T. J. H. Molecular Simulations of the Adsorption of Cycloalkanes in MFI-type Silica. *Phys. Chem. Chem. Phys.* **2005**, *7* (13), 2622−2628.
(32) (a) De Moor, B. A.; Reyniers, M. F.; Gobin, O. C.; Lercher, J. A.; Marin, G. B. Adsorption of C2-C8 *n*-Alkanes in Zeolites. *J. Phys. Chem. C* **2011**, *115* (4), 1204−1219. (b) De Moor, B. A.; Reyniers, M. F.; Marin, G. B. Physisorption and Chemisorption of Alkanes and Alkenes in H-FAU: a Combined Ab Initio-Statistical Thermodynamics

Study. *Phys. Chem. Chem. Phys.* **2009**, *11* (16), 2939−2958. (c) Daems, I.; Leflaive, P.; Methivier, A.; Baron, G. V.; Denayer, J. F. M. Influence of Si: Al-Ratio of Faujasites on the Adsorption of Alkanes, Alkenes and Aromatics. *Microporous Mesoporous Mater.* **2006**, *96* (1−3), 149−156. (d) Askin, A.; Bilgic, C. Thermodynamics of Adsorption of Hydrocarbons on Molecular Sieves NaY and CaY by Inverse Gas Chromatography. *Chem. Eng. J.* **2005**, *112* (1−3), 159−165. (e) Tümsek, F.; İnel, O. Evaluation of the Thermodynamic Parameters for the Adsorption of some n-Alkanes on A Type Zeolite Crystals by Inverse Gas Chromatography. *Chem. Eng. J.* **2003**, *94* (1), 57−66. (f) Denayer, J. F.; Souverijns, W.; Jacobs, P. A.; Martens, J. A.; Baron, G. V. High-Temperature Low-Pressure Adsorption of Branched C-5-C-8 Alkanes on Zeolite Beta, ZSM-5, ZSM-22, zeolite Y, and Mordenite. *J. Phys. Chem. B* **1998**, *102* (23), 4588−4597.

(33) Denayer, J. F. A.; Devriese, L. I.; Couck, S.; Martens, J.; Singh, R.; Webley, P. A.; Baron, G. V. Cage and Window Effects in the Adsorption of n-Alkanes on Chabazite and SAPO-34. *J. Phys. Chem. C* **2008**, *112* (42), 16593−16599.

(34) Denayer, J. F. M.; Ocakoglu, A. R.; Martens, J. A.; Baron, G. V. Investigation of Inverse Shape Selectivity in Alkane Adsorption on SAPO-5 Zeolite Using the Tracer Chromatography Technique. *J. Catal.* **2004**, *226* (1), 240−244.

(35) Peralta, D.; Chaplais, G.; Simon-Masseron, A.; Barthelet, K.; Pirngruber, G. D. Separation of C-6 Paraffins Using Zeolitic Imidazolate Frameworks: Comparison with Zeolite 5A. *Ind. Eng. Chem. Res.* **2012**, *51* (12), 4692−4702.

(36) Elizalde-Gonzalez, M. P.; Ruiz-Palma, R. Gas Chromatographic Characterization of the Adsorption Properties of the Natural Adsorbent CACMM2. *J. Chromatogr., A* **1999**, *845* (1−2), 373−379.

(37) Ohff, A.; Burlakov, V. V.; Rosenthal, U. Isomerization of Olefins by Titanocene and Zirconocene Alkyne Complexes. *J. Mol. Catal A: Chem.* **1996**, *105* (3), 103−110.

(38) Schenk, M.; Vidal, S. L.; Vlugt, T. J. H.; Smit, B.; Krishna, R. Separation of Alkane Isomers by Exploiting Entropy Effects During Adsorption on Silicalite-1: A Configurational-Bias Monte Carlo Simulation Study. *Langmuir* **2001**, *17* (5), 1558−1570.

(39) Wiberg, K. B. The C7−C10 Cycloalkanes Revisited. *J. Org. Chem.* **2003**, *68,* (24), 9322−9329.